

# Simultaneous, Spatially-Resolved Temperature and Velocity Measurements Using Cross-Correlation PIV

by

S. T. Wereley<sup>(1)</sup> and V.P. Hohreiter<sup>(2)</sup>

<sup>(1)</sup>Mechanical Engineering, Purdue University West Lafayette, IN 47907-1288, wereley@purdue.edu

<sup>(2)</sup>Mechanical Engineering, University of Florida, Gainesville, FL, vincenth@ufl.edu

## ABSTRACT

Brownian motion of PIV tracer particles is commonly observed in microfluidics experiments and treated as a source of measurement uncertainty. However, there is information to be gained from this “noise source.” The current work demonstrates an optical technique that uses microscopic particle image velocimetry ( $\mu$ PIV) for temperature measurement. The technique is based on the premise that Brownian motion is a white noise process that will cause broadening of the cross-correlation peak in PIV. Several well-known relationships are available for relating Brownian motion to temperature. A specially modified PIV algorithm detects both the location of the correlation peak to determine velocity as well as the cross sectional area of the peak to calculate the degree of Brownian motion—and thus the temperature. Previously we have demonstrated through experiments and simulations the feasibility of temperature measurements using this technique (Hohreiter, et al., 2002). In the absence of a flow, it was shown that temperatures could be measured with an accuracy near one degree Celsius. The present work considers the effect of fluid movement on the measurement of temperature. The movement of the fluid whose temperature is being measured significantly complicates the technique because spatial gradients in the flow also tend to broaden the correlation peak, masking the effect of temperature on the peak width. A new PIV evaluation algorithm that combines the central difference interrogation and image correction techniques has been developed to address this problem (Wereley and Gui, 2001). The algorithm iteratively adjusts the interrogation window spatial offset while simultaneously deforming the windows to counteract the effect of spatial gradients on the flow. Using this new algorithm, it is possible to infer fluid temperature accurately from the correlation peak width. Alternately, this technique can be thought of as a local viscosity measurement technique if the temperature is known.

## 1. INTRODUCTION

The theoretical basis for the hypothesis of the current work—that temperature measurements can be deduced from the images of individual particles in a flow—rests in the theory of particle diffusion due to Brownian motion. Constant random bombardment by fluid molecules results in a random displacement in the seed-particles. This random particle displacement will be superimposed on any particle displacement due to the fluid velocity. The expression

$$D = KT / 6\pi\mu d_p \quad (1)$$

gives the diffusivity  $D$  of particles of diameter  $d_p$  immersed in a liquid of temperature  $T$  and absolute viscosity  $\mu$ ,  $K$  is Boltzmann’s constant. Noting the dimension of  $D$  is [length<sup>2</sup>/time], the square of the expected distance traveled by a particle with diffusivity  $D$  in some time window  $\Delta t$  is given by

$$\langle s^2 \rangle = 2D\Delta t \quad (2)$$

Combining equations (1) and (2) it is observed that an increase in fluid temperature, with all other factors held constant, will result in a greater expected particle displacement,  $\sqrt{\langle s^2 \rangle}$ . However, absolute viscosity,  $\mu$ , is a function of temperature and so  $\langle s^2 \rangle \propto T/\mu$ . The effect of this relationship depends on the phase of the fluid. For a liquid, increasing temperature decreases absolute viscosity—so the overall effect on the ratio  $T/\mu$  follows the change in  $T$ . For a gas, however, increasing temperature increases absolute viscosity meaning that the effect on  $T/\mu$ , and hence  $\langle s^2 \rangle$ , would need to be determined from fluid specific properties.

Relating changes in fluid temperature to changes in the magnitude of random seed-particle motion due to Brownian motion is the key to measuring temperature using PIV. To demonstrate the feasibility of using PIV for temperature measurement, an analytical model of how the peak width of the spatial cross-correlation varies with relative Brownian motion levels must be developed. This development was begun by Olsen and Adrian (2000) and furthered by Hohreiter, et al. (2002). Only the final equations will be presented here because the argument is quite lengthy.

From an analysis of cross-correlation PIV, Olsen and Adrian found that one effect of Brownian motion on cross-correlation PIV is to increase the correlation peak width,  $\Delta s_o$ —taken as the 1/e diameter of the Gaussian peak. For the case of light-sheet PIV, it was found that

$$\Delta s_{o,a} = \sqrt{2d_e}/\beta \quad (3)$$

when Brownian motion is negligible, to

$$\Delta s_{o,c} = \sqrt{2(d_e^2 + 8M^2\beta^2 D\Delta t)^{1/2}}/\beta. \quad (4)$$

when Brownian motion is significant (note that in any experiment, even one with significant Brownian motion,  $\Delta s_{o,a}$  can be determined by computing the auto-correlation of one of the PIV image pairs). It can be seen that equation (4) reduces to equation (3) in cases where Brownian motion is a negligible contributor to the measurement (i.e., when  $D\Delta t \rightarrow 0$ ). The constant  $\beta$  is a parameter arising from the approximation of the Airy point-response function as a Gaussian function. Adrian and Yao (1985) found a best fit to occur for  $\beta^2=3.67$ .

For the case of volume illumination PIV, the equations for  $\Delta s_o$  have the same form, but because of the variation of  $d_e$  with distance from the focal plane, the  $d_e$  terms, which are constants in equations (3) and (4), are replaced with integrals over the depth of the device.

The difficulty in calculating the integral term for  $d_e$  for volume illumination PIV can be avoided by strategic manipulation of equations (3) and (4). Squaring both equations respectively, taking their difference, and multiplying by the quantity  $\pi/4$  converts the individual peak width (peak diameter for a 3-D peak) expressions to the difference of two correlation peak areas—namely the difference in area between the auto- and cross-correlation peaks. Performing this operation and substituting equation (1) in for  $D$  yields

$$\Delta A = \pi/4 (\Delta s_{o,c}^2 - \Delta s_{o,a}^2) = C_0 (T/\mu) \Delta t \quad (5)$$

where  $C_0$  is the parameter  $2M^2K/3d_p$ .

The expected particle displacement,  $\sqrt{\langle s^2 \rangle}$ , of classical diffusion theory can now be tied to the peak width of the correlation function,  $\Delta s_o$ , or the change in peak area  $\Delta A$  through the diffusivity  $D$  to a function strictly of temperature,  $T/\mu$ .

## 2. CENTRAL DIFFERENCE IMAGE CORRECTION (CDIC) ALGORITHM

Currently, adaptive, discrete window shifting is widely used with the FFT-based correlation algorithm for reducing the evaluation error and with the image pattern tracking algorithms for increasing the spatial resolution. The adaptive window offset method, as typically implemented, can be referred to as a forward difference interrogation (FDI), because the second interrogation window is shifted in the forward direction of the flow an amount equal to the mean displacement of the particle images initially in the first window. Details of the FDI technique are described by Keane and Adrian (1993), Willert (1996), Cowen and Monismith (1997), and Westerweel et al. (1997). Although the adaptive window shifting method leads to significant improvements in the evaluation quality of PIV recordings in many cases, there are still some potentially detrimental bias errors that cannot be avoided with this technique. For instance, in a flow with large spatial gradients, attributing a measurement to the centroid of the first interrogation region (FDI assumption) can lead to significant errors when compared to its proper location—at the centroid of both interrogation regions. A central difference interrogation (CDI) method was developed and explored by Wereley and Meinhart (2000, 2001), to avoid the shortcomings of FDI and increase the accuracy of the PIV measurement. When using CDI, the first and the second interrogation windows are shifted backward and forward, respectively, each by half of the expected particle image displacement. As multi-pass adaptive spatial shifting techniques, both FDI and CDI require some iteration to achieve optimum results. When properly programmed, using CDI does not cost more computation time than FDI. A recent study by Gui and Wereley (2001) indicates that the bias and random errors of the digital PIV recording evaluation can further be reduced by continuously, rather than discretely, shifting the interrogation windows according to preceding iterations. The peak-locking effect is also minimized with this technique. To account for the distortion of PIV image patterns in complex flow measurements, image correction techniques have been developed. The idea of image correction was first presented by Huang et al. (1993). Similar ideas were also applied by others. However, since the image correction was typically a complex and time-consuming procedure, it has not been widely used. In order to accelerate the evaluation, the authors combine a modified image correction method with the FFT-based correlation algorithm, so that the evaluation

error resulting from the image pattern distortion can be effectively reduced with only minimal additional computation time, i.e. a fraction of the regular evaluation time. Named the central difference image correction (CDIC) method in this paper, the new evaluation algorithm combines ideals of central difference interrogation, adaptive continuous window shifting and image correction, and enables a reliable and accurate evaluation of digital PIV recordings. Details are provided in the illustration below.

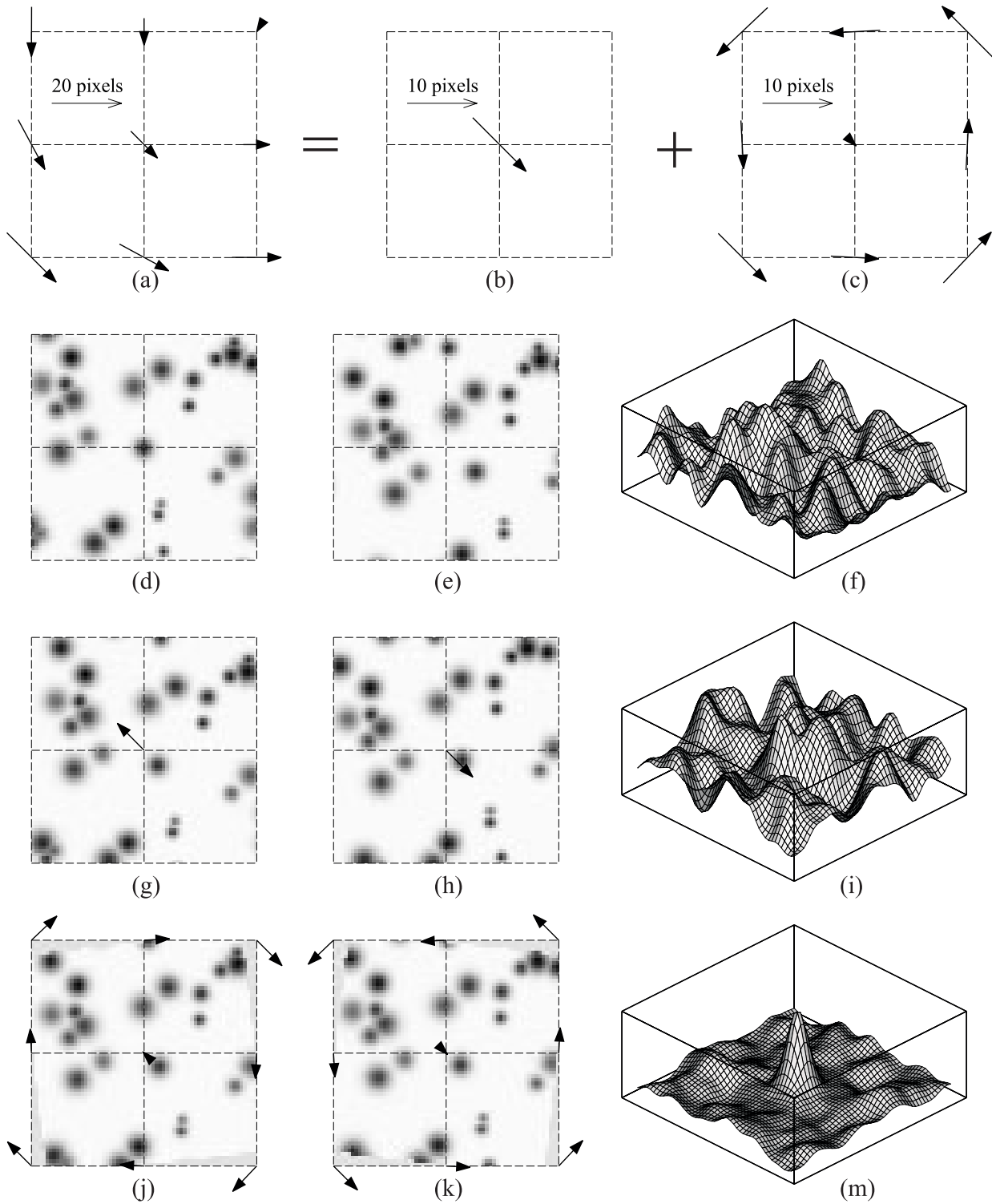


**Fig. 1:** Illustration of interrogation window shift and image pattern correction

The idea of central difference image correction is demonstrated in Fig. 1 by evaluating a synthetic PIV image pair near a strong vortex center with a  $64 \times 64$ -pixel interrogation window and a 50% overlap. The velocity distribution on a small  $3 \times 3$  interrogation grid (Fig. 1a) can be decomposed into a translational movement (Fig. 1b) and distortion (Fig. 1c). When using a traditional cross-correlation algorithm with no window shifting, the evaluation sample pair is obtained with both interrogation windows centered at the evaluation point, e.g. Fig. 1d and 1e for the central point of  $3 \times 3$  grid. The traditional correlation method works well in cases of small particle image displacement and relatively simple flow. But in the current case the image patterns in the sample pair do not match well, so that the correlation function (Fig. 1f) does not show a dominant peak for the particle image displacement. Considering the translation movement of the particle images in the evaluation sample pair, the interrogation windows for the first and second recording can be shifted backwards and forwards, respectively, to realize a central difference interrogation, see Fig. 1g and 1h, so that the image patterns match better to each other. However, the correlation function still does not present a very clear peak to reliably and accurately determine the particle image displacement (Fig. 1i). When considering the particle image distortion, i.e. pre-deforming the image patterns forwards and backward respectively for the first and second evaluation sample (Fig. 1j and 1k) based on the known displacements at the 9 grid points, a very good match of the image patterns is realized, so that a correlation function with a clear main peak is obtained (Fig. 1m). Although in this demonstration the window shifting and the image pattern correction are carried out in two steps, they can be realized in only one step in practical applications.

When using the FFT algorithm to accelerate the calculation, the correlation-based evaluation function is usually written as

$$\Phi(m, n) = \sum_{i=1}^M \sum_{j=1}^N g_1(i, j) \cdot g_2(i+m, j+n) \quad (6)$$

where  $g_1$  and  $g_2$  are gray value distributions of the two evaluation samples, which are restricted in a rectangular interrogation window of size of  $M \times N$  pixels. For traditional correlation algorithms with or without discrete window shifting,  $g_1(i, j)$  and  $g_2(i, j)$  are extracted directly from the discrete gray value distributions of the PIV recording pair  $G_1(i, j)$  and  $G_2(i, j)$ , respectively. However, when using the central difference image correction, the shifts of pixels in the interrogation windows are not limited to discrete integer values and, in most cases, are not constant across the windows. We assume that the displacement of the image pattern at pixel  $(i, j)$  in the interrogation window is determined as  $X(i, j)$  and  $Y(i, j)$ . The following bilinear interpolation function is used for determining the correlated function:

$$g(i, j) = (1-x) \cdot (1-y) \cdot G(i+I, j+J) + x \cdot (1-y) \cdot G(i+I+1, j+J) + y \cdot (1-x) \cdot G(i+I, j+J+1) + x \cdot y \cdot G(i+I+1, j+J+1) \quad (7)$$

wherein  $(I, J)$  and  $(x, y)$  are integer pixels and non-negative sub-pixel values, respectively; for  $g=g_1$  and  $G=G_1$ :  $I+x=-0.5X$ ,  $J+y=-0.5Y$ ; for  $g=g_2$  and  $G=G_2$ :  $I+x=0.5X$ ,  $J+y=0.5Y$ . If  $G(i, j)$  is limited in the  $M \times N$ -pixel sampling window, there may not be enough information to completely fill the rectangular interrogation window, e.g. in Fig. 1j and 1k there are vacancy areas near the edges of the interrogation windows. However, since  $G(i, j)$  is defined in the whole image plane, the interrogation window can be completely filled with PIV recording information in most cases. When the evaluation point is chosen at the edges of the PIV recording, padding or mask techniques (Gui and Merzkirch, 1996, 1998) can be used to deal with the vacancy area problem.

Because the particle image displacement  $(X, Y)$  is unknown before evaluation, initial values are taken to be zero or determined with previous knowledge of the flow. Then the evaluation is iterated until some convergence condition is fulfilled. Instead of determining the particle image displacement  $(X, Y)$  at every pixel in the interrogation window like the conventional image correction methods, displacements at the four corners (4-point method) or also at five center points (9-point method) of the interrogation window are used to determine the correction of the distorted image patterns. For the 4-point method the interrogation window is taken as one rectangular cell, whereas for the 9-point method there are four cells in the interrogation window. Within each rectangular cell, the displacement  $(X, Y)$  is determined with a bilinear interpolation function similar to Eq. (6). This simplification enables not only a fast image-corrected evaluation of the PIV recordings but also good convergence of the multi-pass evaluation algorithm. When using the 4-point image correction method, an adjustment is made, so that the displacement in the window center determines the translation movement and the displacements at the four corners determine the particle image pattern distortion.

The convergence of the CDIC method is tested here using a synthetically generated PIV recording pair with given particle image displacement  $X=5\cos(j/256)$ ,  $Y=5\cos(i/256)$  pixels. The synthetic particle images have a Gaussian gray

value profile and are randomly distributed in PIV recordings of size of  $1024 \times 1024$  pixels. The brightness of the particle image, i.e. the gray value in its center, is 130~250; the particle image diameter at the mid-brightness cross section (FWHM) is 2~5 pixels; the particle image number is 20480, i.e. approximately 20 particles in a  $32 \times 32$ -pixel interrogation window. This PIV recording pair is evaluated by using the above described 4- and 9-point image correction methods, respectively. Convergence factors and evaluation errors expressed as functions of iteration number are given in Fig. 2. The evaluation is conducted with a uniform grid and produces about 4000 displacement vectors. The convergence factor is here defined as a root-mean-square difference between the currently evaluated displacements and the displacements obtained in the previous iteration, whereas the RMS error is the root-mean-square difference between the evaluation results and the given particle image displacements. As shown in Fig. 2a, the evaluation procedures for both the 4-point and 9-point method converge after 6 iterations. Fig. 2b shows that the evaluation with the 4-point method converges at a much lower RMS error than that of the 9-point method. In an ideal case, evaluations are also conducted with given particle image displacements for the image correction without iterations, and the results show that the evaluation error of the 9-point method is somewhat smaller than that of the 4-point. However, the high accuracy of the 9-point method in the ideal case cannot be achieved in practical applications, where the particle image displacements are unknown.

In the above example the CDIC method is combined with the correlation-based interrogation algorithm, i.e. the same interrogation window size is applied to the two evaluation samples. Without any difficulty, the CDIC method can also be combined with the correlation-tracking algorithm, by which the second interrogation window is larger than the first one. As indicated in many previous studies, using the correlation-tracking algorithm is one way to avoid the large evaluation error of the correlation-based interrogation algorithm at large particle image displacements. However, The CDIC method applies a multi-pass continuous window shifting technique, so that the particle image displacement to be determined is near zero after a few iterations. Theoretically the evaluation error of the correlation-based interrogation algorithm is zero at zero displacement (Westerweel et al 1997), and it is usually much smaller than that of the correlation-tracking algorithm when the particle image displacement is within 0.5 pixels (Gui and Merzkirch 2000). In addition, with the same spatial resolution the correlation-tracking algorithm usually costs much more computation time than the correlation-based interrogation algorithm, because the former requires a larger computation window than the latter. Therefore, the combination of the central difference image correction and the correlation-based interrogation algorithm is a better choice. To defend this assertion, a test is conducted with a synthetic PIV recording pair that has the same particle images as in the previous example but smaller amplitude of the particle image displacement, i.e. 3 pixels. This synthetic recording pair is evaluated with combining the CDIC technique with the two correlation algorithms. The RMS evaluation errors at different iteration numbers are provided in Fig. 3. A  $24 \times 24$ -pixel interrogation window is chosen for the correlation-based interrogation, and a padding method is used to enable the FFT acceleration (Gui and Merzkirch 1998). For the correlation tracking the first and second window are  $24 \times 24$  and  $32 \times 32$  pixels, respectively. Test results show that an obviously lower evaluation error is achieved when using the correlation-based interrogation scheme.

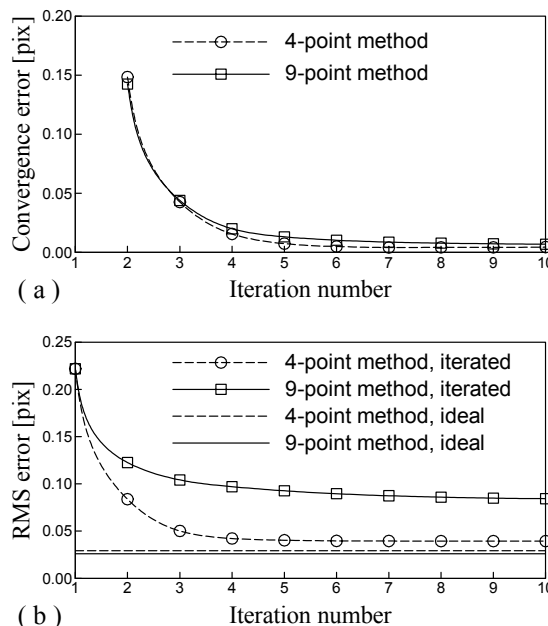


Fig. 2: Convergence of the image correction methods

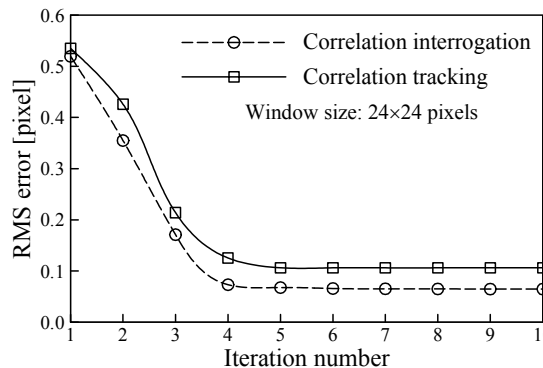
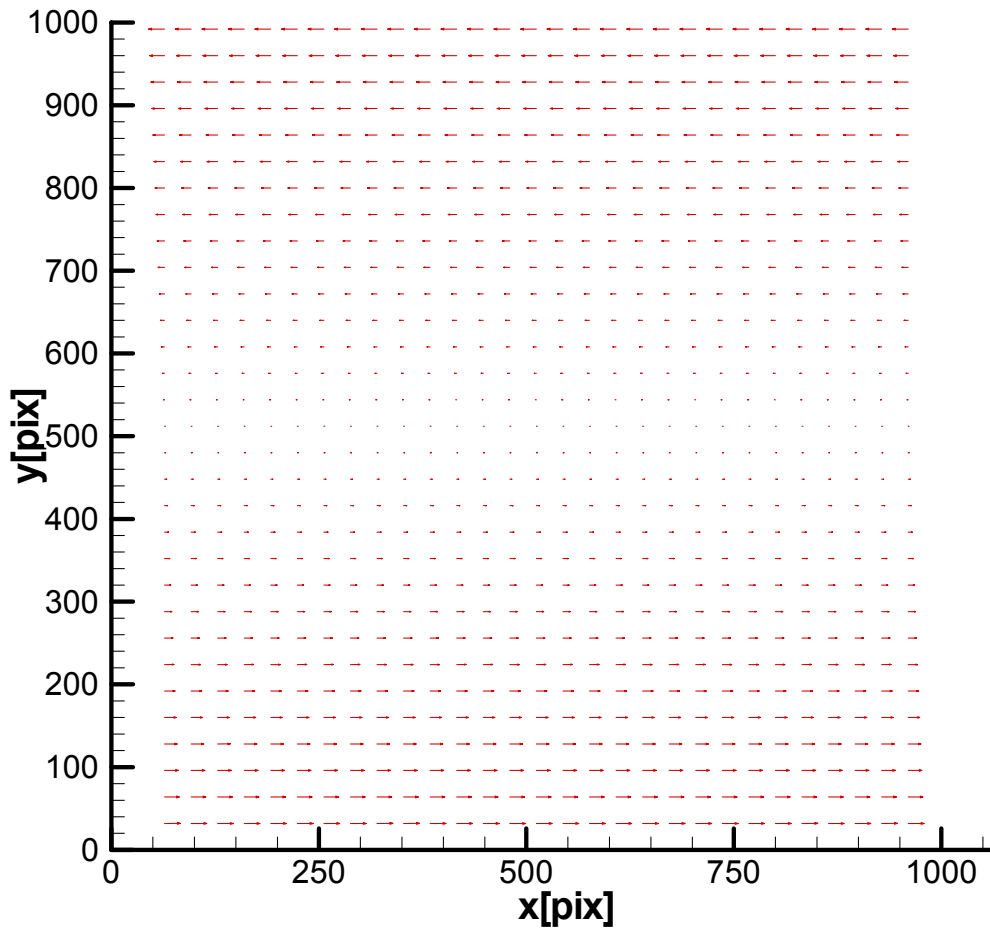


Fig.3: RMS errors of combining the image correction with two different correlation schemes

As indicated in Fig. 2 and 3, four or five iterations are necessary to achieve accurate evaluation results and further increasing the number of iterations will not provide significant improvements. In comparison to the FFT-based discrete window shifting techniques, the new algorithm needs 75% more computation time because of the interpolations. However, because the CDIC is optimally combined with the correlation-based interrogation algorithm, large computation windows can be avoided, so that the computation time may be less than that of the adaptive discrete window shifting technique, as usually applied, in combination with the correlation tracking algorithm.

### 3. FLUID VELOCITY FIELD

Since the spatial gradients in the flow broaden correlation peak, the temperature measurement algorithm must be tested in the presence of spatial gradients to verify that it can work in the presence of spatial gradients. In a general flow, the velocity field and its derivatives will be functions of all three spatial coordinates as well as time. The simplest flow that containing well characterized gradients is a one dimensional shear flow. This flow can be thought of as the zero imposed pressure gradient flow between two parallel planes being translated within their planes relative to each other at a constant rate. This is then a one dimensional flow characterized by a constant shear rate, or a velocity that varies linearly with position. One of the actual velocity fields used is shown in Figure 4 and is characterized by a shear rate of  $0.1 \Delta t^{-1}$ . Lower shear rates were also used.



**Figure 4.** Shear flow velocity field. The longest vectors at the top and bottom of the image measure 50 pixels in length.

As a first step in exploring the possibility of measuring temperature in a flow with gradients in it, the shear flow was simulated using established PIV simulation techniques (Raffel, 1999). The particle image simulation code starts with a  $1024 \times 1024$  pixel black image and creates a number of bright particle images analogous in size (7 pixels) and number density (5000 per image) to an expected experimental particle image (Hohreiter, et al., 2002). The intensity of the simulated particles is given by a Gaussian distribution because a spherical particle image is a convolution of an Airy point-spread function and a geometric particle image—both of which are well-modeled as Gaussian functions. The particles are then displaced according to the imposed velocity field as well as according to the Brownian motion. The

Brownian motion is simulated by a random number generator with zero mean and a normal distribution wherein the standard deviation is given by the expected diffusion distance.

The main difference between the simulated images and experimental  $\mu$ PIV images is that the effects of out-of-focus particles due to volume illumination are not present. Out-of-focus particles negatively contribute to the image by effectively varying the particle image size and intensity, reducing the signal-to-noise ratio, and ultimately affecting the correlation (Meinhart et al., 2000 and Olsen and Adrian, 2000). However, equation (5) demonstrates that these effects, which are present in both the auto-correlation and cross-correlation peak morphology, are removed from consideration by using the difference of the cross-correlation and auto-correlation peak widths to infer temperature. Therefore, even though the simulated images more closely approximate PIV images under light-sheet illumination than volume illumination, they should provide considerable insight into the volume-illumination case.

#### 4. EXTRACTING TEMPERATURE INFORMATION

Using the continuous window shifting and image correction techniques outlined above for processing the simulated images, almost completely eliminated the effects of shear on the correlation peak. Figure 5 shows contour plots of the cross correlation peaks for the cases of using continuous window shifting and image correction (left) and not using the image correction (right) to measure a simulated flow with shear and Brownian motion present. The outermost contour in both plots represents the  $e^{-1}$  height of the peak—the standard deviation. In the left figure, the height of outermost contour is 13.41 pixels and its width is 13.79 pixels, less than 3% change between the two directions. In the right figure, the height of the outermost contour is 13.61 pixels, similar to the left figure, however the width of the contour is 16.04—a change of 15%. Since the temperature measurement depends on the cross sectional area change of the peak between a cross correlation and an autocorrelation, it is important area change not be due to velocity gradients. The image correction technique is essential to the success of the temperature measurement technique.

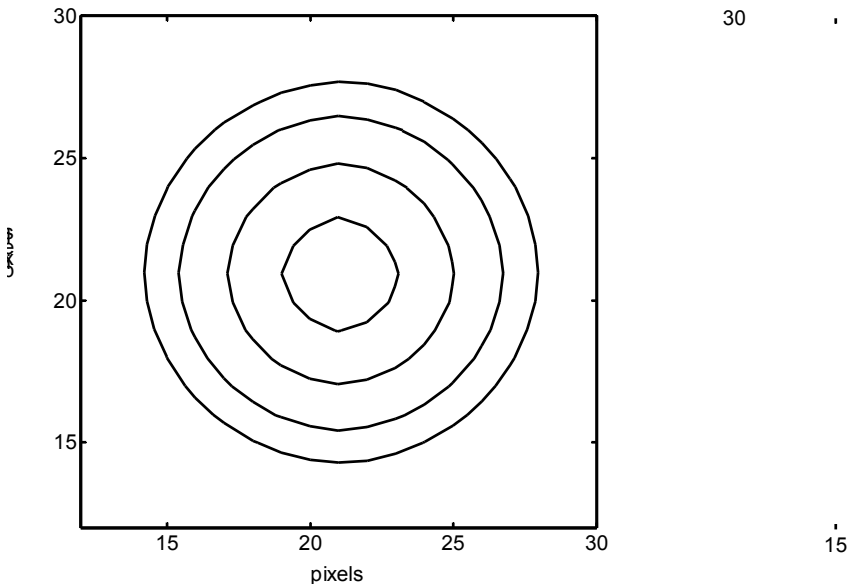


**Figure 5.** Cross correlation of simulated shear flow + Brownian motion images using continuous window shifting and image correction (left) and without using image correction (right). Contours represent 37% ( $e^{-1}$ ), 50%, 70%, and 90% of the peak height.

Since the simulated images are single exposure images, the autocorrelation contains no velocity information, only peak shape information. The cross correlation analysis provides both the velocity and temperature information. Typical peaks are shown in Figure 6.

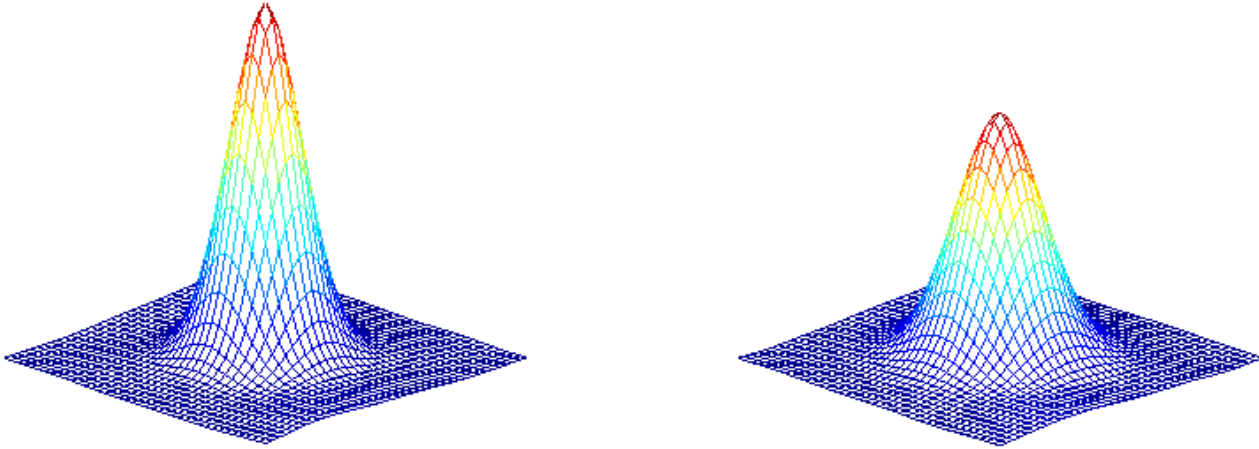


**Figure 6.** Autocorrelation (left) and cross correlation (right) for a typical image set shown on the same scale.

The first step in extracting the temperature information from a pair of images is to correlate each image with itself (i.e. autocorrelate), storing the correlation peaks, to get a measure of the particle image characteristics at each measurement point. Then interrogate the image pair using a cross correlation based scheme to get the local velocity and again store the correlation peaks. A continuous window shifting and image correction algorithm are essential to the success of this step. Next, the correlation peak widths are extracted from both the autocorrelations and the cross correlations at some fraction of the peak height, taken here at the  $e^{-1}$  height. At this point, the area change can be used with Equation 5 to calculate the ratio  $T/\mu$ , provided the calibration constant in that equation is known. The calibration constant can be calculated directly from the properties of the particles and the imaging system, or it can be computed from a known temperature point within the flow—the approach used here. If the composition of the fluid is known, the values of the ratio  $T/m$  directly yield a temperature measurement. If the composition of the fluid is not known, another calibration experiment in which several known temperatures are measured can yield this information. At this point, the process is finished with the fluid’s velocity and temperature successfully measured in a highly spatially-resolved manner. While this technique is described here as being a temperature measurement technique, it can also be thought of as a viscosity measurement technique if the temperature is known.

## 5. RESULTS

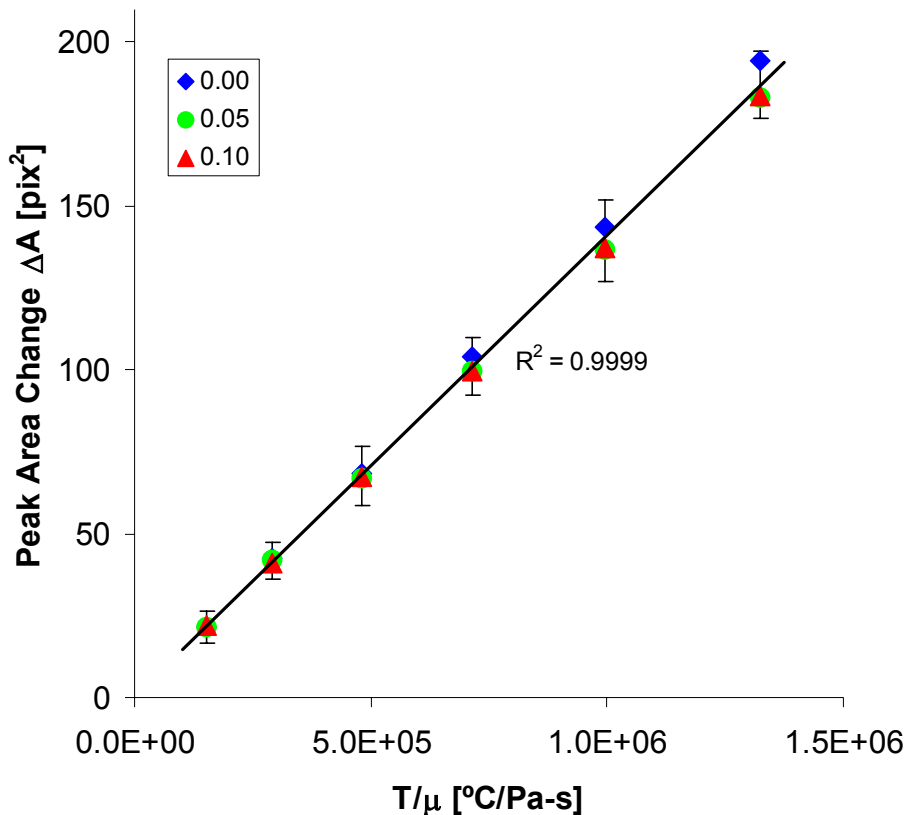
A test matrix consisting of 3 different shear rates (0.00, 0.05, and  $0.10 \Delta t^{-1}$ ) and 6 different temperatures (0, 20, 40, 60, 80, and  $100^\circ\text{C}$ ) was constructed. Flows for each set of operating conditions were simulated and analyzed using the PIV temperature measurement technique as described above. The results are given in Table 1.

Table 1. Results for the temperature calculations

	$0.00 \Delta t^{-1}$			$0.05 \Delta t^{-1}$			$0.10 \Delta t^{-1}$		
$T_{in}$	$\Delta A$	$T/\mu$	$T_{piv}$	$\Delta A$	$T/\mu$	$T_{piv}$	$\Delta A$	$T/\mu$	$T_{piv}$
$^\circ\text{C}$	$\text{pix}^2$	$^\circ\text{C}/\text{Pa}\cdot\text{s}$	$^\circ\text{C}$	$\text{pix}^2$	$^\circ\text{C}/\text{Pa}\cdot\text{s}$	$^\circ\text{C}$	$\text{pix}^2$	$^\circ\text{C}/\text{Pa}\cdot\text{s}$	$^\circ\text{C}$
0	21.6	1.48E+05	-1.4	21.4	1.54E+05	-0.3	21.9	1.58E+05	0.3
20	42.4	2.91E+05	19.8	42.1	3.04E+05	21.3	41.3	2.97E+05	20.6
40	68.6	4.71E+05	39.1	67.1	4.84E+05	40.3	67.4	4.86E+05	40.5
60	104.1	7.14E+05	59.6	99.5	7.18E+05	59.9	99.6	7.17E+05	59.8
80	143.8	9.87E+05	78.7	136.9	9.88E+05	78.8	137.1	9.88E+05	78.8
100	194.2	1.33E+06	99.7	183.2	1.32E+06	99.1	183.6	1.32E+06	99.2

Figure 7 shows the relationship between the peak area change  $\Delta A$  and  $T/\mu$ , which according to Equation 5 should be proportional. The error bars at each temperature indicate the degree of variability of the peak width measurement over all

three sets of data. A line with zero intercept is fitted to all three shear rates together. The fit parameter of the line is  $R^2=0.9999$ , indicating that to within out ability to calculate,  $\Delta A$  and  $T/\mu$  are proportional. Additionally, the three sets of data can be regressed independently to the same degree of proportionality.



**Figure 7.** Proportional relationship between peak area change  $\Delta A$  and  $T/\mu$ .

Once the value of the ratio  $T/\mu$  is established, it is little work to proceed to extracting the temperature. As noted above, if the temperature is known, the viscosity can be extracted. In this work, values of  $T$  and  $\mu$  were entered into a spreadsheet and a  $T/\mu$  column constructed. Then using this table and a lookup feature, the value of the ratio  $T/\mu$  can be directly associated with a temperature. The results of this process are shown in Figure 8 which demonstrate the excellent linearity and temperature resolution of the technique. Averaging over all the temperature measurements made, the RMS difference between the input temperature  $T_{in}$  and the temperature measured by the PIV technique  $T_{piv}$  is  $0.82\text{ }^{\circ}\text{C}$ .

## 6. CONCLUSIONS

The PIV temperature and velocity measurement technique has been shown to work well by using evidence from simulated images. The flows examined were one dimensional shear flows of varying shear rates. The simulated images are idealized images in that they have identical particle sizes and intensities. Comparison of previous simulation results with experimental results indicate that while the idealizations used in the simulations do provide best-case results, the experimental uncertainty is not more than 50% larger than that of the simulations. The present simulations show that temperature can be measured over a large temperature range ( $100\text{ }^{\circ}\text{C}$ ) with an RMS uncertainty of  $0.82\text{ }^{\circ}\text{C}$ . In practice this technique can be expected to deliver uncertainties of approximately  $1.2\text{ }^{\circ}\text{C}$  over a similar temperature range.

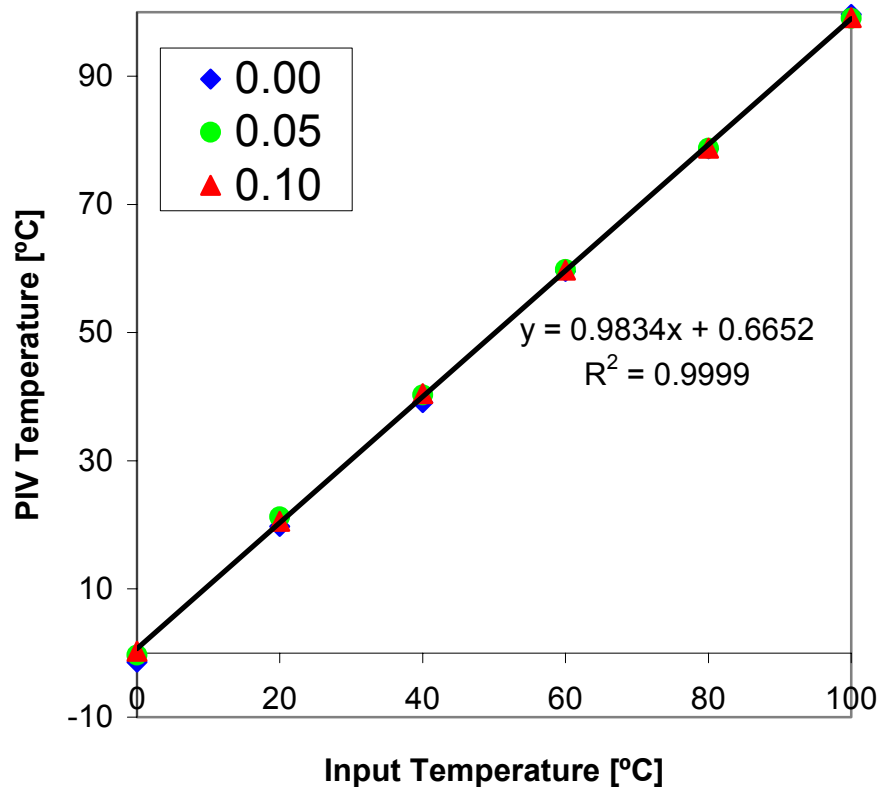


**Figure 8.** Comparison of input temperature  $T_{in}$  and the temperature measured by the PIV technique  $T_{piv}$ .

## 7. REFERENCES

- Adrian RJ, Yao CS** (1985) Pulsed laser technique application to liquid and gaseous flows and the scattering power of seed materials. *Applied Optics*, 24, 44-52.
- Cowen EA; Monismith SG** (1997) A hybrid digital particle tracking velocimetry technique. *Exp Fluids* 22: 199-211.
- Gui L; Merzkirch W** (1996) Phase-separation of PIV digital mask technique. *ERCOFTAC Bulletin* 30: 45-48.
- Gui L; Merzkirch W** (1998) Generating arbitrarily sized interrogation windows for correlation-based analysis of particle image velocimetry recordings. *Exp. Fluids* 24: 66-69.
- Gui L; Merzkirch W** (2000) A comparative study of the MQD method and several correlation-based PIV evaluation algorithms. *Exp. Fluids* 28: 36-44.
- Gui L; Wereley ST** (2002) A correlation-based continuous window shift technique for reducing the peak locking effect in digital PIV image evaluation. *Exp. Fluids* 32: 506-517.
- Hohreiter V; Wereley ST; Olsen M; Chung J** (2002) Cross-correlation analysis for temperature measurement,” *Measurement Science Technology in press*.
- Huang HT; Fiedler HE; Wang JJ** (1993) Limitation and improvement of PIV; Part II: Particle image distortion, a novel technique. *Exp Fluids* 15: 263-273
- Keane RD; Adrian RJ** (1993) Theory and simulation of particle image velocimetry. In: *Laser anemometry advances applications*, 5<sup>th</sup> International Conference, Veldhoven, Netherlands, 23-27 August, Proc SPIE Series, vol 2052, pp 477-492
- Meinhart CD; Wereley ST; Gray MHB** (2000) Volume illumination for two-dimensional particle image velocimetry. *Meas. Sci. Tech.* 11: 809-814.
- Olsen MG and Adrian RJ** (2000) Brownian motion and correlation in particle image velocimetry, *Opt. Laser Technol.* 32, 621-7.
- Raffel M; Willert C.; Kompenhans J** (1998) *Particle Image Velocimetry*. Springer-Verlag, 1998.
- Wereley ST; Gui L** (2001) PIV measurement in a four-roll-mill flow with a central difference image correction (CDIC) method,” 4th International Symposium on Particle Image Velocimetry, Paper 1027, Göttingen, Germany, Sept.

**Wereley ST; Meinhart CD** (2000), Accuracy improvements in particle image velocimetry, *10<sup>th</sup> International Symposium on "Applications of Laser Techniques to fluid Mechanics"*, Lisbon, Portugal, July

**Wereley ST; Meinhart CD** (2001) Second-Order Accurate Particle Image Velocimetry. *Exp. Fluids*. 31:258-268.

**Westerweel J; Dabiri D; Gharib M** (1997), The effect of a discrete window offset on the accuracy of cross-correlation analysis of digital PIV recordings, *Exp. Fluids* 23, 20-28

**Willert CE** (1996) The fully digital evaluation of photographic PIV recordings. *Appl. Sci. Res.* 56, 79-102